Analyst

PAPER

View Article Online
View Journal | View Issue

Cite this: *Analyst*, 2021, **146**, 2152

Fluorescence sensing of cyanide anions based on Au-modified upconversion nanoassemblies†

Chunning Sun * and Michael Gradzielski *

Cyanides have been recognized as one of the most toxic chemicals and are harmful to the environment and human beings. Herein, fluorescence resonance energy transfer (FRET)-based upconversion nanoprobes for cyanide anions have been designed and prepared by assembling Au nanoparticles (NPs) on core–shell-structured $NaYF_4$:Yb,Er@$NaYF_4$:Yb upconversion NPs (csUCNPs), where csUCNPs act as the energy donor and Au NPs act as the energy acceptor. The Au content was optimized in order to have a large quenching efficiency in upconversion luminescence (UCL). The cyanide-mediated redox reaction leads to the consumption of Au NPs, resulting in UCL recovery by the inhibition of the FRET process. On the basis of these features, csUCNP/Au nanoassemblies can serve as sensitive nanoprobes for cyanide ions with a detection limit of 1.53 μM. Moreover, no significant UCL variation was observed upon the addition of other interfering ions, showing the excellent selectivity of nanoprobes toward cyanide ion sensing. The easy preparation of such upconversion-based nanoprobes provides a promising platform for sensitive and selective sensing of other hazardous species.

Received 30th September 2020,
Accepted 26th January 2021

DOI: 10.1039/d0an01954b

rsc.li/analyst

Introduction

Unlike toxic metal cations, causing severe damage by virtue of their accumulative feature in organs, cyanide is a well-known hazardous anionic species, which can strongly interact with cytochrome c oxidase, resulting in the failure of oxygen transport to the mitochondria and leading to the death of human beings and aquatic life within minutes by affecting the central nervous system even at a low concentration.[1] Accordingly, the World Health Organization (WHO) limits the acceptable level of cyanide up to 1.9 μM in drinking water.[2] In spite of its highly lethal toxicity, nearly 1.4 million tons of cyanide are produced every year, as it is widely used in industry,[3] such as polymer and fiber manufacturing, gold mining, electroplating, and metallurgy. In consequence, unexpected cyanide leakage will seriously contaminate the groundwater and drinking water.[4] Thus, considerable attention has been given to cyanide detection, and sensitive and selective sensing techniques for cyanide at low levels are highly desired.

To date, numerous analytical techniques including electrochemical,[5,6] voltammetric,[7] chromatographic,[8] and surface-enhanced Raman spectroscopy (SERS) strategies[9,10] have been developed for the sensing of cyanide ions. Although high accuracy can be achieved by these approaches in quantitative analyses, complicated instruments and time-consuming procedures are usually required. Owing to the high sensitivity, easy operation, and applicability in biosensing, fluorescent chemodosimeters have been widely investigated.[11,12] Unlike traditional fluorescent materials excited by ultraviolet (UV) or visible light, upconversion chromophores possess different luminescence mechanisms, which are capable of converting near-infrared (NIR) excitation to visible or UV light when co-doped with appropriate activator ions.[13] They feature large anti-Stokes shifts, sharp and narrow multicolor emissions, high chemical stability, and relatively low toxicity. Moreover, the use of NIR light as the excitation wavelength not only enables higher penetration depth but also avoids the biomolecular autofluorescence and background interference.[14] Hence, upconversion-based nanophosphors have attracted increasing interest in the sensing field.[15] Generally, the Förster resonance energy transfer (FRET) process is employed for the upconversion-based fluorescence sensing of analytes. Up to now, a number of functional materials have been coupled to upconversion NPs to achieve sensing properties, such as organic dyes,[16–23] metal–ligand complexes,[24–26] carbon nanomaterials,[27–30] noble metals,[31–33] quantum dots,[34–36] and two-dimensional materials.[37–40] Fluorescent chemosensors based on upconversion NPs have been designed for the detection of cyanide ions as well. However, the commonly used organic dyes and metal–ligand complexes, acting as energy

Stranski-Laboratorium für Physikalische und Theoretische Chemie, Institut für Chemie, Technische Universität Berlin, Strasse des 17. Juni 124, 10623 Berlin, Germany. E-mail: sunchunning@gmail.com, michael.gradzielski@tu-berlin.de

†Electronic supplementary information (ESI) available: XRD results of OA-UCNPs and OA-csUCNPs, FT-IR OA-, ligand-free, and PEI-csUCNPs, TEM images and UV-vis absorption spectra of csUCNP/Au nanoassemblies with different contents of Au NPs. See DOI: 10.1039/d0an01954b

acceptors, suffer from either photobleaching or complex synthetic processes.[41–43]

In this contribution, we report the facile design and synthesis of nanocomposites through assembling Au nanoparticles (NPs) on the surface of core–shell-structured $NaYF_4$:Yb,Er@$NaYF_4$:Yb upconversion NPs (abbreviated as csUCNPs). Au-modified csUCNP nanoassemblies (abbreviated as csUCNP/Au) can be applied as fluorescent nanoprobes for cyanide anions based on the FRET mechanism, where csUCNPs act as the energy donor and Au NPs act as the energy acceptor. Moreover, the content of the Au NPs was optimized to achieve maximum quenching efficiency in upconversion luminescence (UCL). The cyanide-mediated redox reaction oxidizes Au into $[Au(CN)_2]^-$ in the absence and presence of other interfering ions, leading to the consumption of Au NPs, inhibiting the FRET process, and thus resulting in the recovery of UCL emissions. Accordingly, these features enable the sensitive and selective sensing of cyanide ions.

Experimental

Materials

Yttrium(III) acetate tetrahydrate (99.9%), ytterbium(III) acetate hydrate (99.9%), and erbium(III) acetate hydrate (99.9%) were purchased from Alfa Aesar. Oleic acid (OA, 90%), 1-octadecene (ODE, 90%), ammonium fluoride (NH_4F, ≥98%), sodium hydroxide (NaOH, ≥98%), methanol (99.8%), ethanol (≥99.8%), *N*,*N*-dimethylformamide (DMF, 99.8%), cyclohexane (99.5%), formic acid (≥98%), tetrachloroauric(III) acid trihydrate ($HAuCl_4{\cdot}3H_2O$, ≥99.9%), tetrakis(hydroxymethyl)phosphonium chloride (THPC, 80% in H_2O), NaCN (≥95%), and polyethylenimine (PEI, branched, M_w ~25 000) were obtained from Sigma-Aldrich. Milli-Q water (18.2 MΩ cm at 25 °C) was used in all experiments.

Characterization

Fourier transform infrared (FT-IR) spectra were acquired with a Thermo Scientific Nicolet iS5 FT-IR spectrometer using the KBr method. The spectra were recorded in transmission mode in a wavenumber range from 4000 to 500 cm^{-1}. UV-Vis absorption spectra were obtained by using a CARY 50 spectrophotometer. Transmission electron microscopy (TEM) and energy-dispersive X-ray spectroscopy (EDS) were performed with a FEI Tecnai G^2 20 S-TWIN electron microscope with a LaB_6 cathode operating at 200 kV. Powder X-ray diffraction (XRD) spectra were obtained by using a Philips X'Pert MPD Pro X-ray diffractometer at a scanning rate of 4° min^{-1} in a 2θ range from 10° to 90° with Cu Kα radiation (λ = 0.15406 nm). ζ-Potential and dynamic light scattering (DLS) measurements were carried out with an Anton Paar Litesizer™ 500. UCL emission spectra were collected at room temperature with a fiber-coupled spectrometer (Ocean HDX, Ocean Optics) equipped with an external 980 nm laser (Roithner Lasertechnik GmbH) with a power of 3 W.

Synthesis of Au NPs

Au NPs were synthesized as described previously.[44] Typically, 12 μL of THPC and 0.25 mL of NaOH (2.0 M) were added to 45 mL of water, and then the mixture was stirred vigorously for 5 min followed by a quick injection of 2 mL of $HAuCl_4$ solution (1 wt%). The color changed to dark brown immediately. This solution was stored in a dark container and stirred overnight.

Synthesis of OA-UCNPs

The synthesis of oleate-capped $NaYF_4$:Yb,Er NPs (abbreviated as OA-UCNPs) was carried out by a high-temperature coprecipitation method according to a previous publication with minor modifications.[45] Typically, 3.12 mL of $Y(CH_3COO)_3$ (0.2 M), 0.8 mL of $Yb(CH_3COO)_3$ (0.2 M) and 0.8 mL of $Er(CH_3COO)_3$ (0.02 M) aqueous solutions were added to a three-neck flask containing 6 mL of OA and 14 mL of ODE at room temperature. The mixed solution was heated to 110 °C for 30 min to remove the water, followed by heating to 160 °C for 40 min to form lanthanide-oleate complexes and then cooled down to 50 °C. A methanol solution (10 mL) containing NH_4F (3.2 mmol) and NaOH (2.0 mmol) was added afterward and stirred at 50 °C for 30 min. After evaporating the methanol, the solution was heated to 305 °C at a ramp rate of 10 °C min^{-1} and maintained at this temperature for 45 min under a N_2 atmosphere. After cooling down to room temperature, OA-UCNPs were precipitated out by adding excess ethanol, collected by centrifugation at 6000 rpm for 5 min, repeatedly washed with ethanol, and finally redispersed in cyclohexane.

Synthesis of core–shell-structured OA-csUCNPs

Oleate-capped $NaYF_4$:Yb,Er@$NaYF_4$:Yb (abbreviated as OA-csUCNPs) core–shell-structured upconversion NPs were prepared by coating a similar material on the core OA-UCNPs.[46] Typically, $Y(CH_3COO)_3$ (3.2 mL, 0.2 M) and $Yb(CH_3COO)_3$ (0.8 mL, 0.2 M) were added into a three-neck flask containing 6 mL of OA and 14 mL of ODE at room temperature. The mixed solution was heated to 110 °C for 30 min to remove the water, followed by heating to 160 °C for 40 min to form lanthanide-oleate complexes and then cooled down to room temperature. The above-synthesized OA-UCNPs dispersed in cyclohexane were added to the flask. The solution was heated to 110 °C to remove the cyclohexane and then subsequently cooled down to room temperature. A methanol solution (10 mL) containing NH_4F (3.2 mmol) and NaOH (2.0 mmol) was added afterward and stirred at 50 °C for 30 min. After heating to 110 °C to evaporate the methanol, the solution was heated to 305 °C at a ramp rate of 10 °C min^{-1} and maintained at that temperature for 45 min under a N_2 atmosphere. After letting the solution to cool down to room temperature, OA-csUCNPs were precipitated out by the addition of excess ethanol, collected by centrifugation at 6000 rpm for 5 min, washed with ethanol several times, and finally redispersed in cyclohexane.

Preparation of ligand-free UCNPs and csUCNPs

Ligand-free upconversion NPs were prepared *via* a vortexing method according to our previous publication.[47] Formic acid (5 mmol) was added to 2 mL of cyclohexane solution containing OA-UCNPs (10 mg mL^{-1}) directly; the mixture was then shaken for 10 s (3000 rpm) on a vortex mixer, and ligand-free UCNPs were precipitated out. The resultant NPs were obtained by centrifugation at 6000 rpm for 20 min, washed once with ethanol and three times with water, and finally redispersed in water. Ligand-free csUCNPs were obtained similar to bare UCNPs, except that OA-csUCNPs in cyclohexane solution were employed.

Preparation of csUCNP/Au nanoassemblies

For this purpose, 20 mg of bare csUCNPs were dispersed in 4 mL of H_2O containing 40 mg of PEI (pH ~10), followed by overnight stirring. PEI-modified csUCNPs (abbreviated as PEI-csUCNPs) were obtained *via* centrifugation at 10 000 rpm for 20 min, washed three times with water, and finally redispersed in water and the pH was adjusted to 5. csUCNP/Au nanoassemblies were prepared by the addition of appropriate freshly prepared Au NPs to a solution containing PEI-csUCNPs (the content of the csUCNPs was fixed at 0.5 mg mL^{-1}) and ultrasonicated for 10 min. Assuming the diameters of the Au NPs and the csUCNPs to be 1.7 and 43 nm, respectively, we can estimate that ~140 Au NPs decorate one csUCNP for 0.10 mM Au content. The resulting csUCNP/Au nanocomposites were then collected by centrifugation at 9000 rpm for 30 min, washed with water several times, and redispersed in DMF/H_2O (5/1, v/v) solution. This solvent mixture was employed as in pure water the system becomes a bit turbid due to agglomeration processes.

Procedures for cyanide ion sensing

The sensing of CN^- was performed by adding different amounts of CN^- solution to the csUCNP/Au nanocomposites in DMF/H_2O (5/1, v/v) solution; the concentration of the csUCNPs was kept at 0.5 mg mL^{-1}, and the concentration of CN^- ranged from 0 to 280 μM. Selectivity experiments were performed by the addition of 2 mM of other ions with a similar procedure. The UCL spectra of the resulting samples were recorded under the excitation of a 3 W 980 nm laser.

Results and discussion

Design principle for cyanide anion sensing

The design strategy of a csUCNP/Au nanosystem for selective cyanide anion sensing relies on the FRET process, where core–shell-structured upconversion NPs are used as the energy donor and Au NPs are employed as the energy acceptor, as shown in Fig. 1a. Without modification, csUCNPs give rise to green and red luminescence emissions deriving from the $^2H_{11/2} \rightarrow {}^4I_{15/2}$, $^4S_{3/2} \rightarrow {}^4I_{15/2}$, and $^4F_{9/2} \rightarrow {}^4I_{15/2}$ transitions of Er^{3+} under 980 nm laser excitation. Ultrasmall Au NPs (diameter of *ca.* 1.7 nm) with a broad absorption in the whole visible region exhibit quenching rather than the plasmonic effect. When the csUCNPs couple with Au NPs, an efficient FRET process occurs, resulting in the weakening of green and red emissions in the UCL intensity. However, the energy transfer from csUCNPs to Au NPs is suppressed in the presence of cyanide ions, owing to the etching property of cyanide ions for Au NPs. As a consequence, the UCL of csUCNPs is recovered by the consumption of Au NPs upon the addition of cyanide ions (Fig. 1b), and the variation in the UCL intensity of csUCNP/Au nanoassemblies allows the quantitative detection of cyanide ions.

Characterization of csUCNPs/Au nanoassemblies

Hydrophobic oleate-capped UCNPs were first prepared by employing OA as the ligand *via* a high-temperature coprecipitation method.[45] The TEM image shows that the core UCNPs have a uniform hexagonal morphology with an average diameter of about 35 nm (Fig. 2a), and the average diameter of the hexagonal csUCNPs increases to approximately 43 nm with uniformity maintained, suggesting the successful growth of the shell on the core NPs (Fig. 2b). Additionally, the XRD pat-

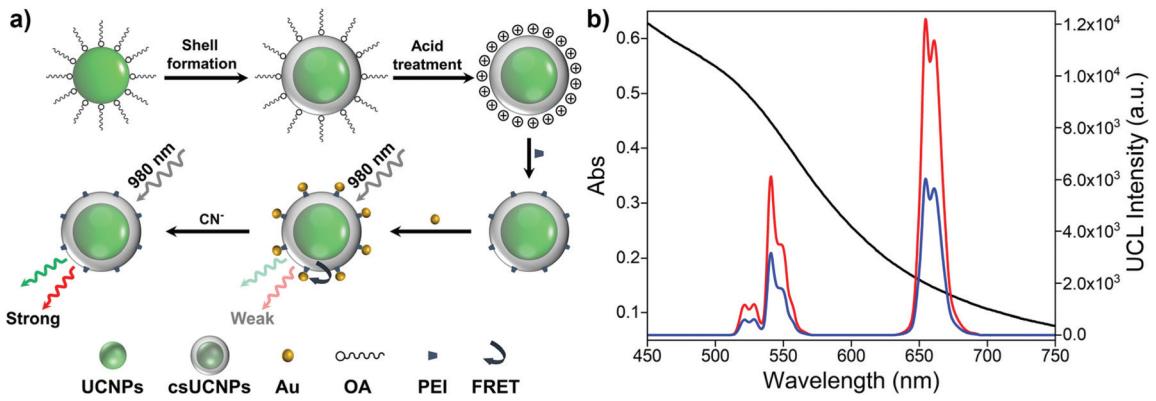

Fig. 1 (a) Schematic illustration of the synthesis of csUCNP/Au nanoassemblies and their response to cyanide ions. (b) UV-vis spectrum of Au NPs (black) and UCL spectra of csUCNPs/Au in the absence (blue) and presence (red) of cyanide ions.

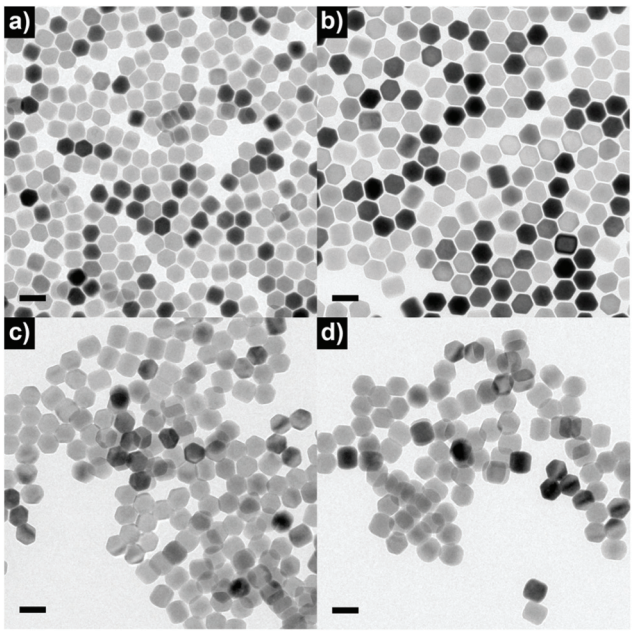

Fig. 2 TEM images of (a) OA-UCNPs, (b) OA-csUCNPs, (c) ligand-free csUCNPs, and (d) PEI-csUCNPs. Scale bars: 50 nm.

terns of the core-only UCNPs and core–shell-structured csUCNPs, which are in excellent agreement with the pure hexagonal phase (JCPDS file number 28-1192), demonstrate high crystallinity with well-defined diffraction peaks (Fig. S1†). After the treatment of OA-UCNPs with formic acid, the oleate ligand can be easily removed.[47] The obtained ligand-free csUCNPs can be well-dispersed in water to form a stable colloidal solution, and the zeta potential was determined to be 36.8 mV (pH ~5.5). Moreover, these well-dispersed bare csUCNPs favor the attachment of PEI on their surface. As revealed by TEM images, the particle size and morphology are retained after ligand removal and further polymer functionalization (Fig. 2c and d).

Additionally, FT-IR measurements were performed to characterize ligand removal and subsequent PEI attachment (Fig. S2†). Two strong transition bands centered at 2923 and 2854 cm^{-1} are clearly observed in the OA-csUCNP sample, which can be assigned to the asymmetric and symmetric stretching vibrations of methylene groups in the long alkyl chain, and a weak peak at 3008 cm^{-1}, assigned to the =C–H stretching vibration, is shown in the spectrum. Moreover, the two peaks centered at 1561 and 1460 cm^{-1} can be assigned to the asymmetric and symmetric stretching vibrations of the carboxylate group. These characteristic peaks validate the presence of the oleate ligand on the surface of csUCNPs. However, these characteristic peaks vanish after the formic acid treatment, except for the broad band of solvated water molecules centered at around 3420 cm^{-1}, proving the success in surface ligand removal by acid treatment and confirming the hydrophilic nature of the obtained ligand-free csUCNPs. After polymer functionalization, two bands centered at 2930 and 2854 cm^{-1} appear, which can be attributed to the asymmetric and symmetric stretching vibrations of the C–H bond, respectively. Furthermore, a weak peak centered at 1167 cm^{-1} attributed to the stretching vibrations of the C–N bond and a strong transition band centered at 1545 cm^{-1} attributed to N–H bending vibrations can be observed, thereby revealing the attachment of PEI on the surface of bare csUCNPs.

To obtain csUCNP/Au nanoassemblies, ultrasmall Au NPs with a mean diameter of about 1.7 nm were prepared (Fig. 3a), and the nanocomposites could then be easily generated by assembling negatively charged (−2.7 mV) Au NPs onto the positively charged PEI-csUCNPs (34.3 mV) through electrostatic interactions, as confirmed by TEM (Fig. 3b). As the connection between csUCNP and Au relies on electrostatic interactions, the nonuniform distribution of Au NPs is likely caused by the drying process during the sample preparation for the TEM measurement, as during drying the concentration of the Au NPs increases and therefore their tendency for clustering increases. Compositional analysis of hybrid NPs by EDS shows the presence of Na, F, Y, Yb, and Au elements (Fig. 3c), further evidencing the presence of Au NPs. The hydrodynamic radius of 0.5 mg mL^{-1} csUCNP/Au (0.1 mM Au NPs) nanocomposites remained stable at ~135 nm for a period of at least

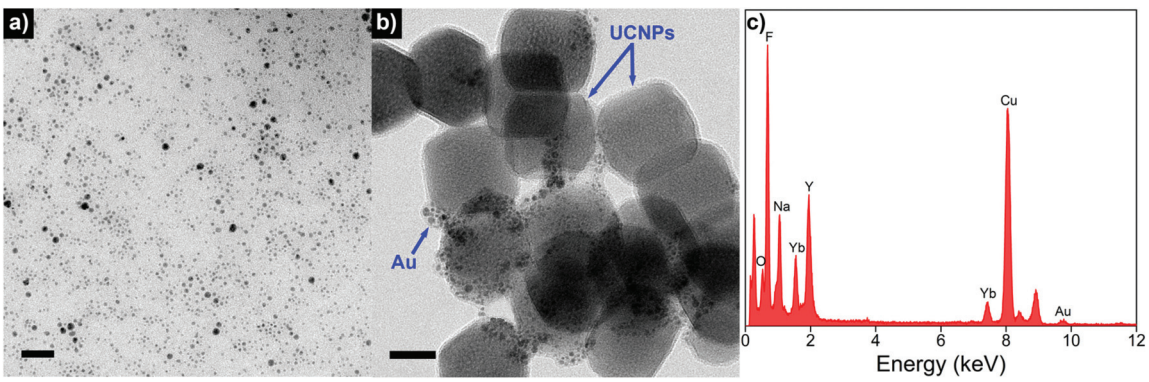

Fig. 3 TEM images of (a) Au NPs and (b) csUCNP/Au nanoassemblies. Scale bars: 20 nm. (c) EDS spectrum of csUCNP/Au nanoassemblies.

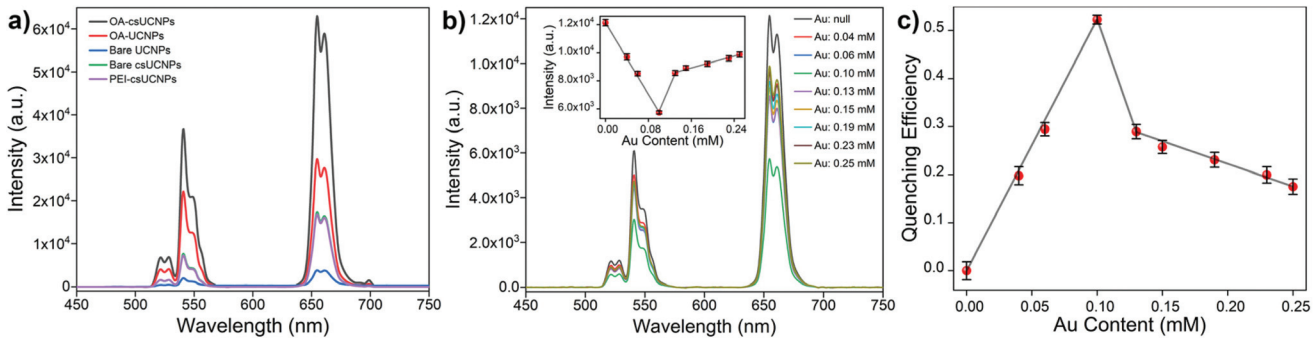

Fig. 4 (a) UCL spectra of OA-UCNPs and OA-csUCNPs dispersed in cyclohexane, bare UCNPs, bare csUCNPs, and PEI-csUCNPs dispersed in water with a concentration of 1 mg mL^{-1} under 3 W 980 nm excitation. (b) UCL spectra of 0.5 mg mL^{-1} csUCNPs upon the addition of different contents of Au NPs. Inset: Variations of UCL intensity at 655 nm upon the addition of Au NPs. (c) Relationship between the fluorescence quenching efficiency of csUCNP/Au nanoassemblies in the 600–700 nm range and the Au content. The black line serves as a guide to the eye. Error bars represent the standard deviations of three independent measurements.

14 days (Fig. S3†), exhibiting excellent stability of the nanocomposites dissolved in the mixed solution.

Next, the optical properties of the csUCNP and csUCNP/Au nanocomposites are investigated. The UCL emission spectra of hydrophobic OA- and ligand-free upconversion NPs under 980 nm laser excitation are shown in Fig. 4a, presenting a relatively low UCL intensity of the OA-UCNPs due to the energy loss by large surface defects.[48] Here a remarkable loss of green and red emissions in UCL intensity is seen in aqueous solution after the transition of OA-UCNPs to ligand-free ones *via* ligand exfoliation by formic acid, attenuated by water molecules.[49,50] In order to enhance the UCL intensity of upconversion NPs, especially hydrophilic ones, core–shell-structured OA-csUCNPs were prepared *via* the same synthetic procedure by coating a similar material on core OA-UCNPs,[46] and bare csUCNPs were obtained *via* the same vortexing method. The UCL intensity of OA-csUCNPs increases by a factor of two compared with the core-only OA-UCNPs in cyclohexane, whereas the UCL intensity of bare csUCNPs is about 4.5 times larger than that of core-only ligand-free UCNPs in aqueous solution, owing to passivated surface defects by the shell layer. Meanwhile, nearly identical UCL emissions of PEI- and bare csUCNPs are observed.

Fluorescence quenching ability of Au NPs to csUCNPs

The optical properties of Au NPs were assessed by UV–vis absorption spectroscopy. Au NPs show a broad absorption band in the visible region. The broad spectral absorbance of Au NPs overlaps well with the UCL of csUCNPs in the green and red regions, as shown in Fig. 1b, enabling efficient FRET between csUCNPs and Au NPs. Furthermore, the FRET process is verified by the phenomenon of UCL reduction in csUCNPs/Au upon 980 nm laser activation.

To optimize the nanosystem, different contents of Au NPs were used to modify PEI-csUCNPs. The performance of different amounts of Au NPs on PEI-UCNPs is evaluated from UCL spectra, which are shown in Fig. 4b. The UCL intensity experiences a significant decrease at the beginning and reaches a minimum when a 0.1 mM Au NP solution is added. However, at higher Au content this trend suddenly stops, and an increase in UCL intensity occurs when the content of Au NPs goes beyond 0.1 mM. Subsequently, a gradual upturn in UCL intensity occurs upon further increasing the Au NP content. In addition, the energy transfer efficiency between

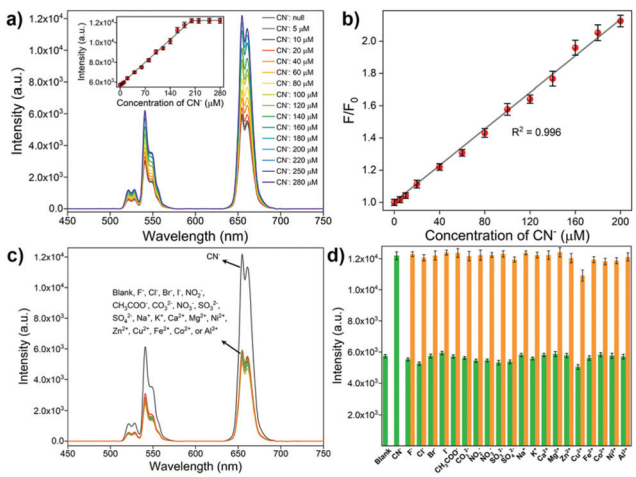

Fig. 5 (a) UCL spectra of 0.5 mg mL^{-1} csUCNPs/Au (0.1 mM Au NPs) upon the addition of different concentrations of cyanide ions. Inset: UCL intensity at 655 nm as a function of the cyanide ion concentration. (b) Linear relationship between the UCL enhancement factor (F/F_0) at 655 nm and the concentration of cyanide ions, where F_0 and F are the luminescence intensities of nanoprobes at 655 nm in the absence and presence of cyanide ions, respectively. (c) UCL spectra of 0.5 mg mL^{-1} csUCNP/Au nanocomposites in the presence of various anions. (d) Changes in UCL intensity of 0.5 mg mL^{-1} csUCNP/Au at 655 nm upon the addition of 200 μM CN^- and 2 mM other ions. Green bars represent the UCL changes upon the addition of various ions, and the orange bars represent the subsequent addition of 200 μM CN^- to the above solution. Error bars represent the standard deviations of three independent measurements.

csUCNPs and Au NPs (*i.e.*, quenching efficiency) is calculated from the UCL emission intensities in the red region (600–700 nm) using the following equation:

$$\eta = 1 - \mathrm{rUCL}/\mathrm{rUCL}_0$$

where η denotes the quenching efficiency in the red region, and rUCL and rUCL_0 are the integrated red emission intensities of csUCNPs/Au and csUCNPs, respectively, in a 600–700 nm range.

As shown in Fig. 4c, the UCL quenching efficiency in a wavelength range of 600–700 nm experiences a substantial increase for a low loading amount of Au NPs, and the greatest quenching efficiency of about 52% is reached upon the addition of 0.1 mM Au NPs. For higher Au content, the quenching efficiency decreases with the increasing content of Au NPs. This abnormal phenomenon for the high loading amount of Au NPs may be attributed to the partial aggregation of Au NPs on csUCNPs, leading to the plasmonic enhancement effect.

In order to verify the aforementioned conjecture, TEM and UV-vis absorption measurements of csUCNP/Au nanocomposites were performed. Obviously, TEM images show that no apparent aggregation of Au NPs takes place for low amounts of added Au NPs (Fig. S4a–c†). In contrast, small agglomerates appear when 0.13 mM Au NPs are added, and the agglomerates become larger with the increasing loading amount of Au NPs (Fig. S4d–h†). Moreover, no obvious absorption peak is observed when the added amount of Au NPs is less than or equal to 0.1 mM. However, an absorption peak at about 535 nm appears when the additive amount of Au NPs is greater than 0.1 mM, and the absorption intensity at 535 nm increases with the growing addition of Au NPs to PEI-csUCNP solutions, indicating the increasing amount of Au aggregates (Fig. S4i†). As a consequence, the competition of the Au-aggregation-induced plasmonic enhancement effect[51] and single ultrasmall Au NP-induced quenching effect results in the uptrend of the UCL intensity in csUCNP/Au nanoassemblies with a high content of Au NPs.

Sensitive and selective detection of cyanide ions

The sensing ability of csUCNP/Au nanoassemblies is based on the recovery of UCL emissions *via* the consumption of Au NPs by the addition of cyanide ions, attributed to the cyanide-mediated oxidation reaction of Au into $[Au(CN)_2]^-$, as described by the following equation:

$$4Au + 8CN^- + O_2 + 2H_2O \rightarrow 4[Au(CN)_2]^- + 4OH^-$$

The csUCNP/Au nanoassemblies formed by the addition of 0.1 mM Au NPs are applied for the sensing of cyanide ions due to their sufficient fluorescence quenching efficiency. As discussed above, the consumption of Au NPs occurs upon the addition of cyanide ions, resulting in the suppression of the FRET process and corresponding to a gradual increase of UCL intensity in all emissions, as shown in Fig. 5a. No further variation of UCL intensity is observed after the addition of 2 equiv. of cyanide ions, as expected from the reaction equation. The variations of the fluorescence enhancement factor at 655 nm (F/F_0, where F_0 and F refer to the luminescence intensities of nanoprobes at 655 nm in the absence and presence of cyanide ions, respectively) *versus* the addition of cyanide ions are shown in Fig. 5b. The calibration curve exhibits a linear relationship between F/F_0 and the concentration of cyanide ions in a range from 0 to 200 μM, and the linear correlation coefficient of the calibration curve is 0.996. The limit of detection (LOD) for cyanide is calculated to be 1.53 μM according to the 3σ rule. Compared to the developed methods for cyanide ion sensing (Table 1), the sensitivity of the UCNP/Au nanocomposites is well competitive.

To further assess the selectivity of the nanosystem for cyanide ions, a series of control experiments was performed to investigate the response of csUCNPs/Au toward other potentially interfering ions. As shown in Fig. 5c, only the addition of cyanide ions leads to a noticeable variation in UCL, but no obvious UCL changes are observed upon the addition of other ions, such as F^-, Cl^-, Br^-, I^-, CH_3COO^-, CO_3^{2-}, NO_2^-, NO_3^-, SO_3^{2-}, SO_4^{2-}, Na^+, K^+, Ca^{2+}, Mg^{2+}, Zn^{2+}, Cu^{2+}, Fe^{2+}, Ni^{2+}, Co_2^+, and Al^{3+}. In addition, competition experiments were carried out by adding cyanide anions to solutions of csUCNPs/Au in the presence of other ions. Significant enhancements of the UCL intensity are observed upon the addition of cyanide ions, as shown in Fig. 5d. Therefore, it can be stated that csUCNP/Au nanoassemblies can act as highly sensitive and selective fluorescence nanoprobes for cyanide ion sensing.

Table 1 Comparison of various methods for cyanide ion sensing

Materials	Methods	Linear range	LOD	Ref.
Gold nanocluster	Fluorometry	0–10 μM	0.2 μM	12
Iridium-complex-modified UCNPs	Fluorometry	0–1.8 mM	62.6 μM	42
Phenothiazine-cyanine-modified UCNPs	Colorimetry	0–50 μM	9.85 μM	43
	Fluorometry	0–300 uM	0.84 μM	43
Bicinchoninic acid–Cu(II) complex	Colorimetry	0–50 mM	1.25 μM	52
Co(II)Pc modified carbon paste electrode	Voltammetry	24–270 μM	3.6 μM	53
Chitosan–gold nanoparticle	Colorimetry	0–38 μM	2.31 μM	54
Hexaazatriphenylene	Electrochemical assay	0–200 μM	0.87 μM	55
csUCNP/Au nanocomposites	Fluorometry	0–200 μM	1.53 μM	This work

Conclusions

In summary, we have developed a facile approach to prepare csUCNP/Au nanoassemblies for cyanide ion sensing based on the FRET process, where csUCNPs act as the energy donor and Au NPs act as the energy acceptor. For this purpose, the optimum Au NP loading content was determined with the aim of achieving the highest fluorescence quenching efficiency. Au NPs are exclusively etched by cyanide ions but are inert to other ions, and the cyanide-induced Au consumption favors the inhibition of the FRET process, leading to the recovery of the UCL emissions. Competition experiments show that the response of csUCNP/Au nanoassemblies toward cyanide ions remains undisturbed by the presence of other interfering ions. This means that the method presented here allows for the selective sensing of cyanide ions in the presence of other ions with high sensitivity (1.53 μM). Such a cyanide-mediated FRET process may be extended to the future design of other upconversion-based analysts.

Author contributions

C. Sun and M. Gradzielski conceived the concepts. C. Sun conducted the experiments and analysed the data. M. Gradzielski supervised the entire process, and both authors discussed the results and jointly wrote the manuscript.

Conflicts of interest

The authors declare no competing financial interest.

Acknowledgements

C. Sun acknowledges the financial support from the China Scholarship Council (CSC, No. 201404910463) and TU Berlin. The authors are grateful to Ina Speckmann and Jan Ron Justin Simke for the XRD and TEM measurements, respectively.

Notes and references

1 Z.-Z. Dong, C. Yang, K. Vellaisamy, G. Li, C.-H. Leung and D.-L. Ma, *ACS Sens.*, 2017, **2**, 1517–1522.
2 K. Deng, L. Wang, Q. Xia, R. Liu and J. Qu, *Sens. Actuators, B*, 2019, **296**, 126645.
3 J. Ma and P. K. Dasgupta, *Anal. Chim. Acta*, 2010, **673**, 117–125.
4 R. R. Dash, A. Gaur and C. Balomajumder, *J. Hazard. Mater.*, 2009, **163**, 1–11.
5 Y. G. Timofeyenko, J. J. Rosentreter and S. Mayo, *Anal. Chem.*, 2007, **79**, 251–255.
6 G. Ding, H. Zhou, J. Xu and X. Lu, *Chem. Commun.*, 2014, **50**, 655–657.
7 A. Safavi, N. Maleki and H. R. Shahbaazi, *Anal. Chim. Acta*, 2004, **503**, 213–221.
8 M. Tomasulo, S. Sortino, A. J. P. White and F. M. Raymo, *J. Org. Chem.*, 2006, **71**, 744–753.
9 D. Senapati, S. S. R. Dasary, A. K. Singh, T. Senapati, H. Yu and P. C. Ray, *Chem. – Eur. J.*, 2011, **17**, 8445–8451.
10 G. Liu, W. Cai, L. Kong, G. Duan, Y. Li, J. Wang and Z. Cheng, *J. Hazard. Mater.*, 2013, **248–249**, 435–441.
11 R. Badugu, J. R. Lakowicz and C. D. Geddes, *J. Am. Chem. Soc.*, 2005, **127**, 3635–3641.
12 Y. Liu, K. Ai, X. Cheng, L. Huo and L. Lu, *Adv. Funct. Mater.*, 2010, **20**, 951–956.
13 M. Haase and H. Schäfer, *Angew. Chem., Int. Ed.*, 2011, **50**, 5808–5829.
14 S. Gai, C. Li, P. Yang and J. Lin, *Chem. Rev.*, 2014, **114**, 2343–2389.
15 G.-R. Tan, M. Wang, C.-Y. Hsu, N. Chen and Y. Zhang, *Adv. Opt. Mater.*, 2016, **4**, 984–997.
16 N. Wang, X. Yu, K. Zhang, C. A. Mirkin and J. Li, *J. Am. Chem. Soc.*, 2017, **139**, 12354–12357.
17 R. Wei, Z. Wei, L. Sun, J. Z. Zhang, J. Liu, X. Ge and L. Shi, *ACS Appl. Mater. Interfaces*, 2016, **8**, 400–410.
18 J. Peng, W. Xu, C. L. Teoh, S. Han, B. Kim, A. Samanta, J. C. Er, L. Wang, L. Yuan, X. Liu and Y.-T. Chang, *J. Am. Chem. Soc.*, 2015, **137**, 2336–2342.
19 Y. Zhou, W. Pei, C. Wang, J. Zhu, J. Wu, Q. Yan, L. Huang, W. Huang, C. Yao, J. S. C. Loo and Q. Zhang, *Small*, 2014, **10**, 3560–3567.
20 C. Li, J. Liu, S. Alonso, F. Li and Y. Zhang, *Nanoscale*, 2012, **4**, 6065–6071.
21 Y. Zhou, W. Pei, X. Zhang, W. Chen, J. Wu, C. Yao, L. Huang, H. Zhang, W. Huang, S. C. J. Loo and Q. Zhang, *Biomaterials*, 2015, **54**, 34–43.
22 J. Peng, C. L. Teoh, X. Zeng, A. Samanta, L. Wang, W. Xu, D. Su, L. Yuan, X. Liu and Y.-T. Chang, *Adv. Funct. Mater.*, 2016, **26**, 191–199.
23 M. K. Mahata and K. T. Lee, *Nanoscale Adv.*, 2019, **1**, 2372–2381.
24 Q. Liu, J. Peng, L. Sun and F. Li, *ACS Nano*, 2011, **5**, 8040–8048.
25 X. Li, Y. Wu, Y. Liu, X. Zou, L. Yao, F. Li and W. Feng, *Nanoscale*, 2014, **6**, 1020–1028.
26 Y. Liu, A. Jiang, Q. Jia, X. Zhai, L. Liu, L. Ma and J. Zhou, *Chem. Sci.*, 2018, **9**, 5242–5251.
27 L. Wu, J. Wang, M. Yin, J. Ren, D. Miyoshi, N. Sugimoto and X. Qu, *Small*, 2014, **10**, 330–336.
28 C. Zhang, Y. Yuan, S. Zhang, Y. Wang and Z. Liu, *Angew. Chem., Int. Ed.*, 2011, **50**, 6851–6854.
29 C. Liu, Z. Wang, H. Jia and Z. Li, *Chem. Commun.*, 2011, **47**, 4661–4663.
30 P. Vilela, A. El-Sagheer, T. M. Millar, T. Brown, O. L. Muskens and A. G. Kanaras, *ACS Sens.*, 2016, **2**, 52–56.
31 Y. Xiao, L. Zeng, T. Xia, Z. Wu and Z. Liu, *Angew. Chem., Int. Ed.*, 2015, **54**, 5323–5327.
32 X. Chen, J. Wang, C. Yang, Z. Ge and H. Yang, *Sens. Actuators, B*, 2017, **255**, 1316–1324.

33 M. Wang, W. Hou, C.-C. Mi, W.-X. Wang, Z.-R. Xu, H.-H. Teng, C.-B. Mao and S.-K. Xu, *Anal. Chem.*, 2009, **81**, 8783–8789.
34 L. Liu, R. Li, G. Wang, Z. Gu and Z. Li, *Sens. Actuators, B*, 2019, **285**, 453–461.
35 H. Kurt, M. Yüce, B. Hussain and H. Budak, *Biosens. Bioelectron.*, 2016, **81**, 280–286.
36 L. Xu, J. Liu, L. Pei, Y. Xu and Z. Xia, *J. Mater. Chem. C*, 2019, **7**, 6112–6119.
37 Y. Cen, J. Tang, X.-J. Kong, S. Wu, J. Yuan, R. Yu and X. Chu, *Nanoscale*, 2015, **7**, 13951–13957.
38 R. Deng, X. Xie, M. Vendrell, Y.-T. Chang and X. Liu, *J. Am. Chem. Soc.*, 2011, **133**, 20168–20171.
39 J. Yuan, Y. Cen, X.-J. Kong, S. Wu, C.-L. Liu, R.-Q. Yu and X. Chu, *ACS Appl. Mater. Interfaces*, 2015, **7**, 10548–10555.
40 Y. Yuan, S. Wu, F. Shu and Z. Liu, *Chem. Commun.*, 2014, **50**, 1095–1097.
41 J. Liu, Y. Liu, Q. Liu, C. Li, L. Sun and F. Li, *J. Am. Chem. Soc.*, 2011, **133**, 15276–15279.
42 L. Yao, J. Zhou, J. Liu, W. Feng and F. Li, *Adv. Funct. Mater.*, 2012, **22**, 2667–2672.
43 S. Zhao, F. Wu, Y. Zhao, Y. Liu and L. Zhu, *J. Photochem. Photobiol., A*, 2016, **319–320**, 53–61.
44 D. G. Duff, A. Baiker and P. P. Edwards, *Langmuir*, 1993, **9**, 2301–2309.
45 Z. Li and Y. Zhang, *Nanotechnology*, 2008, **19**, 345606.
46 F. Wang, R. Deng, J. Wang, Q. Wang, Y. Han, H. Zhu, X. Chen and X. Liu, *Nat. Mater.*, 2011, **10**, 968–973.
47 C. Sun, J. R. J. Simke and M. Gradzielski, *Mater. Adv.*, 2020, **1**, 1602–1607.
48 F. Wang, J. Wang and X. Liu, *Angew. Chem., Int. Ed.*, 2010, **49**, 7456–7460.
49 R. Arppe, I. Hyppanen, N. Perala, R. Peltomaa, M. Kaiser, C. Wurth, S. Christ, U. Resch-Genger, M. Schaferling and T. Soukka, *Nanoscale*, 2015, **7**, 11746–11757.
50 F. T. Rabouw, P. T. Prins, P. Villanueva-Delgado, M. Castelijns, R. G. Geitenbeek and A. Meijerink, *ACS Nano*, 2018, **12**, 4812–4823.
51 L. Polavarapu, J. Pérez-Juste, Q.-H. Xu and L. M. Liz-Marzán, *J. Mater. Chem. C*, 2014, **2**, 7460–7476.
52 A. A. Biradar, A. V. Biradara, T. Sun, Y. Chan, X. Huang and T. Asefa, *Sens. Actuators, B*, 2016, **222**, 112–119.
53 E. Figueira, L. Neres, M. Ruy, G. Troiano and M. D. Sotomayor, *Anal. Methods*, 2016, **8**, 6353–6360.
54 C. Radhakumary and K. Sreenivasan, *Analyst*, 2012, **137**, 5387–5391.
55 G. Men, W. Han, C. Chen, C. Liang and S. Jiang, *Analyst*, 2019, **144**, 2226–2230.